Baryon interactions from lattice QCD with physical masses — strangeness $S = -1$ sector —

Hidekatsu Nemura[1,2,⋆], *Sinya* Aoki[2,3,4], *Takumi* Doi[2,5], *Shinya* Gongyo[2], *Tetsuo* Hatsuda[2,5], *Yoichi* Ikeda[1,2], *Takashi* Inoue[2,6], *Takumi* Iritani[2], *Noriyoshi* Ishii[1,2], *Takaya* Miyamoto[2,3], and *Kenji* Sasaki[2,3]

[1] *Research Centre for Nuclear Physics, Osaka University, Osaka, 567-0047, Japan*
[2] *Theoretical Research Division, Nishina Centre, RIKEN, Saitama, 351-0198, Japan*
[3] *Centre for Gravitational Physics, Yukawa Institute for Theoretical Physics, Kyoto University, Kyoto, 606-8502, Japan*
[4] *Centre for Computational Sciences, University of Tsukuba, Tsukuba 305-8577, Japan*
[5] *iTHEMS Program and iTHES Research Group, RIKEN, Saitama, 351-0198, Japan*
[6] *Nihon University, College of Bioresource Sciences, Kanagawa 252-0880, Japan*

Abstract. We present our recent results of baryon interactions with strangeness $S = -1$ based on Nambu-Bethe-Salpeter (NBS) correlation functions calculated from lattice QCD with almost physical quark masses corresponding to $(m_\pi, m_K) \approx (146, 525)$ MeV and large volume $(La)^4 = (96a)^4 \approx (8.1 \text{ fm})^4$. In order to perform a comprehensive study of baryon interactions, a large number of NBS correlation functions from NN to ΞΞ are calculated simultaneously by using large scale computer resources. In this contribution, we focus on the strangeness $S = -1$ channels of the hyperon interactions by means of HAL QCD method. Four sets of three potentials (the ${}^3S_1 - {}^3D_1$ central, ${}^3S_1 - {}^3D_1$ tensor, and the ${}^1S_0$ central potentials) are presented for the $\Sigma N - \Sigma N$ (the isospin $I = 3/2$) diagonal, the $\Lambda N - \Lambda N$ diagonal, the $\Lambda N \to \Sigma N$ transition, and the $\Sigma N - \Sigma N$ ($I = 1/2$) diagonal interactions. Scattering phase shifts for ΣN ($I = 3/2$) system are presented.

1 Introduction

Nuclear force and strangeness nuclear forces provide an important starting point to understand how hypernuclei are bound, in which hyperons (or strange quarks) are embedded in normal nuclei as "impurities"[1]. Determining how such a baryon-baryon interaction is described from a fundamental perspective is a challenging problem in physics. Although a normal nucleus is successfully described by utilising the high precision nucleon-nucleon (NN) potentials together with a three-nucleon force a quantitatively same-level description of a hypernucleus is still difficult because of large uncertainties of hyperon-nucleon (YN) and hyperon-hyperon (YY) interactions; those YN and YY potentials are not well constrained from experimental data due to the short life time of hyperons. A recent experimental study shows a tendency to repulsive Σ-nucleus interaction and only a four-body Σ-hypernucleus (${}^4_\Sigma$He) has been observed; those suggests a repulsive nature of the ΣN interaction. It has been pointed out that

⋆Speaker, e-mail: hidekatsu.nemura@rcnp.osaka-u.ac.jp

a $\Lambda N - \Sigma N$ coupled-channel interaction accompanied with ${}^3S_1 - {}^3D_1$ mixing by tensor operator plays a vital role to have a hypernucleus being bound[2]. Such quantitative understanding is useful to study properties of hyperonic matters inside the neutron stars, where recent observations of massive neutron star heavier than $2M_\odot$ [3, 4] may be issued against a hyperonic equation of state (EOS) employed in such a study. Furthermore, better understanding of YN and YY is becoming increasingly important due to the observation of the binary neutron star merger[5, 6].

During the last decade a new lattice QCD approach to study a hadron-hadron interaction has been proposed[7, 8] and developed to overcome the numerical difficulty[9]. In this approach, the interhadron potential is obtained by means of the lattice QCD measurement of the Nambu-Bethe-Salpeter (NBS) wave function. The observables such as the phase shifts and the binding energies are calculated by using the resultant potential[10]. A large scale lattice QCD calculation is now in progress[11] to study the baryon interactions from NN to $\Xi\Xi$ by measuring the NBS wave functions for 52 channels from the 2 + 1 flavor lattice QCD. See also Ref.[12] for the study of $\Omega\Omega$ interaction.

The purpose of this report is to present our recent results of the $\Lambda N - \Sigma N$ (both the isospin $I = 1/2, 3/2$) systems using full QCD gauge configurations. Several earlier results had already been reported at LATTICE 2008, LATTICE 2009 and LATTICE 2011[13] with heavier quark masses and smaller lattice volumes. Although the possibility of "mirage" is pointed out[14], calculations with larger quark masses for the $\Sigma^- n$ channel are found in Ref.[15]. This report shows the latest results of those studies, based on recent works reported at LATTICE 2013[16, 17]; the baryon-baryon interaction in the strangeness $S = -1$ sector (i.e, $\Lambda N - \Lambda N$, $\Lambda N - \Sigma N$, and $\Sigma N - \Sigma N$ (both $I = 1/2$ and $3/2$)) is studied at almost physical quark masses corresponding to $(m_\pi, m_K) \approx (146, 525)$MeV and large volume $(La)^4 = (96a)^4 \approx (8.1\ \text{fm})^4$.

2 Outline of the HAL QCD method

In order to study the baryon-baryon interactions, we first define the equal time NBS wave function in particle channel $\lambda = \{B_1, B_2\}$ with Euclidean time t [7, 8]

$$\phi_{\lambda E}(\vec{r})\mathrm{e}^{-Et} = \sum_{\vec{X}} \left\langle 0 \left| B_{1,\alpha}(\vec{X} + \vec{r}, t) B_{2,\beta}(\vec{X}, t) \right| B = 2, E, S, I \right\rangle, \tag{1}$$

where $B_{1,\alpha}(x)$ ($B_{2,\beta}(x)$) denotes the local interpolating field of baryon B_1 (B_2) with mass m_{B_1} (m_{B_2}), and $E = \sqrt{k_\lambda^2 + m_{B_1}^2} + \sqrt{k_\lambda^2 + m_{B_2}^2}$ is the total energy in the centre of mass system of a baryon number $B = 2$, strangeness S, and isospin I state. For $B_{1,\alpha}(x)$ and $B_{2,\beta}(x)$, we employ the local interpolating field of octet baryons given by

$$\begin{array}{llll} p = \varepsilon_{abc}\,(u_a C\gamma_5 d_b)\,u_c, & n = -\varepsilon_{abc}\,(u_a C\gamma_5 d_b)\,d_c, & \Sigma^+ = -\varepsilon_{abc}\,(u_a C\gamma_5 s_b)\,u_c, & \Sigma^- = -\varepsilon_{abc}\,(d_a C\gamma_5 s_b)\,d_c, \\ \Sigma^0 = \frac{1}{\sqrt{2}}\,(X_u - X_d), & \Lambda = \frac{1}{\sqrt{6}}\,(X_u + X_d - 2X_s), & \Xi^0 = \varepsilon_{abc}\,(u_a C\gamma_5 s_b)\,s_c, & \Xi^- = -\varepsilon_{abc}\,(d_a C\gamma_5 s_b)\,s_c, \\ \text{where} & X_u = \varepsilon_{abc}\,(d_a C\gamma_5 s_b)\,u_c, & X_d = \varepsilon_{abc}\,(s_a C\gamma_5 u_b)\,d_c, & X_s = \varepsilon_{abc}\,(u_a C\gamma_5 d_b)\,s_c. \end{array} \tag{2}$$

For simplicity, we have suppressed the explicit spinor indices and spatial coordinates in Eq. (2) and the renormalisation factors in Eq. (1). Based on a set of the NBS wave functions, we define a non-local potential $\left(\frac{\nabla^2}{2\mu_\lambda} + \frac{k_\lambda^2}{2\mu_\lambda}\right)\delta_{\lambda\lambda'}\phi_{\lambda' E}(\vec{r}) = \int d^3r'\ U_{\lambda\lambda'}(\vec{r}, \vec{r'})\phi_{\lambda' E}(\vec{r'})$ with the reduced mass $\mu_\lambda = m_{B_1} m_{B_2}/(m_{B_1} + m_{B_2})$.

In lattice QCD calculations, we compute the four-point correlation function defined by[9]

$$F_{\alpha\beta,JM}^{\langle B_1 B_2 \overline{B_3 B_4}\rangle}(\vec{r}, t - t_0) = \sum_{\vec{X}} \left\langle 0 \left| B_{1,\alpha}(\vec{X} + \vec{r}, t) B_{2,\beta}(\vec{X}, t) \overline{\mathcal{J}_{B_3 B_4}^{(J,M)}(t_0)} \right| 0 \right\rangle, \tag{3}$$

where $\overline{\mathcal{J}^{(J,M)}_{B_3B_4}(t_0)} = \sum_{\alpha'\beta'} P^{(J,M)}_{\alpha'\beta'} \overline{B_{3,\alpha'}(t_0)B_{4,\beta'}(t_0)}$ is a source operator that creates B_3B_4 states with the total angular momentum J, M. The normalised four-point function can be expressed as

$$R^{\langle B_1B_2\overline{B_3B_4}\rangle}_{\alpha\beta,JM}(\vec{r}, t-t_0) = \mathrm{e}^{(m_{B_1}+m_{B_2})(t-t_0)} F^{\langle B_1B_2\overline{B_3B_4}\rangle}_{\alpha\beta,JM}(\vec{r}, t-t_0)$$
$$= \sum_n A_n \sum_{\vec{X}} \left\langle 0 \left| B_{1,\alpha}(\vec{X}+\vec{r},0)B_{2,\beta}(\vec{X},0) \right| E_n \right\rangle \mathrm{e}^{-(E_n-m_{B_1}-m_{B_2})(t-t_0)} + O(\mathrm{e}^{-(E_{\mathrm{th}}-m_{B_1}-m_{B_2})(t-t_0)}), \quad (4)$$

where E_n ($|E_n\rangle$) is the eigen-energy (eigen-state) of the six-quark system and $A_n = \sum_{\alpha'\beta'} P^{(JM)}_{\alpha'\beta'}$ $\langle E_n|\overline{B}_{4,\beta'}\overline{B}_{3,\alpha'}|0\rangle$. Hereafter, the spin and angular momentum subscripts are suppressed for F and R for simplicity. At moderately large $t-t_0$ where the inelastic contribution above the pion production $O(\mathrm{e}^{-(E_{\mathrm{th}}-m_{B_1}-m_{B_2})(t-t_0)}) = O(\mathrm{e}^{-m_\pi(t-t_0)})$ becomes negligible, we can construct the non-local potential U through $\left(\frac{\nabla^2}{2\mu_\lambda} + \frac{k^2_\lambda}{2\mu_\lambda}\right)\delta_{\lambda\lambda'}F_{\lambda'}(\vec{r}) = \int d^3r'\, U_{\lambda\lambda'}(\vec{r},\vec{r}')F_{\lambda'}(\vec{r}')$. In lattice QCD calculations in a finite box, it is practical to use the velocity (derivative) expansion, $U_{\lambda\lambda'}(\vec{r},\vec{r}') = V_{\lambda\lambda'}(\vec{r},\vec{\nabla}_r)\delta^3(\vec{r}-\vec{r}')$. In the lowest few orders we have

$$V(\vec{r},\vec{\nabla}_r) = V^{(0)}(r) + V^{(\sigma)}(r)\vec{\sigma}_1\cdot\vec{\sigma}_2 + V^{(T)}(r)S_{12} + V^{(^{LS}_{ALS})}(r)\vec{L}\cdot(\vec{\sigma}_1 \pm \vec{\sigma}_2) + O(\nabla^2), \quad (5)$$

where $r = |\vec{r}|$, $\vec{\sigma}_i$ are the Pauli matrices acting on the spin space of the i-th baryon, $S_{12} = 3(\vec{r}\cdot\vec{\sigma}_1)(\vec{r}\cdot\vec{\sigma}_2)/r^2 - \vec{\sigma}_1\cdot\vec{\sigma}_2$ is the tensor operator, and $\vec{L} = \vec{r}\times(-i\vec{\nabla})$ is the angular momentum operator. The first three-terms constitute the leading order (LO) potential while the fourth term corresponds to the next-to-leading order (NLO) potential. By taking the non-relativistic approximation, $E_n - m_{B_1} - m_{B_2} \simeq \frac{k^2_{\lambda,n}}{2\mu_\lambda} + O(k^4_{\lambda,n})$, and neglecting the V_{NLO} and the higher order terms, we obtain $\left(\frac{\nabla^2}{2\mu_\lambda} - \frac{\partial}{\partial t}\right)R_{\lambda\varepsilon}(\vec{r},t) \simeq V^{(\mathrm{LO})}_{\lambda\lambda'}(\vec{r})\theta_{\lambda\lambda'}R_{\lambda'\varepsilon}(\vec{r},t)$, with $\theta_{\lambda\lambda'} = \mathrm{e}^{(m_{B_1}+m_{B_2}-m_{B'_1}-m_{B'_2})(t-t_0)}$. Note that we have introduced the matrix form $R_{\lambda'\varepsilon} = \{R_{\lambda'\varepsilon_0}, R_{\lambda'\varepsilon_1}\}$ with linearly independent NBS wave functions $R_{\lambda'\varepsilon_0}$ and $R_{\lambda'\varepsilon_1}$. For the spin singlet state, we extract the central potential as $V^{(Central)}_{\lambda\lambda'}(r; J=0) = (\theta_{\lambda\lambda'})^{-1}(R^{-1})_{\varepsilon'\lambda'}(\frac{\nabla^2}{2\mu_\lambda} - \frac{\partial}{\partial t})R_{\lambda\varepsilon'}$. For the spin triplet state, the wave function is decomposed into the S- and D-wave components as

$$\begin{cases} R(\vec{r};\,^3S_1) = \mathcal{P}R(\vec{r}; J=1) \equiv \frac{1}{24}\sum_{\mathcal{R}\in O}\mathcal{R}R(\vec{r}; J=1), \\ R(\vec{r};\,^3D_1) = \mathcal{Q}R(\vec{r}; J=1) \equiv (1-\mathcal{P})R(\vec{r}; J=1). \end{cases} \quad (6)$$

Therefore, the Schrödinger equation with the LO potentials for the spin triplet state becomes

$$\begin{Bmatrix}\mathcal{P}\\ \mathcal{Q}\end{Bmatrix}\times\left\{V^{(0)}_{\lambda\lambda'}(r)+V^{(\sigma)}_{\lambda\lambda'}(r)+V^{(T)}_{\lambda\lambda'}(r)S_{12}\right\}\theta_{\lambda\lambda'}R_{\lambda'\varepsilon}(\vec{r},t-t_0)=\begin{Bmatrix}\mathcal{P}\\ \mathcal{Q}\end{Bmatrix}\times\left\{\frac{\nabla^2}{2\mu_\lambda}-\frac{\partial}{\partial t}\right\}R_{\lambda\varepsilon}(\vec{r},t-t_0), \quad (7)$$

from which the central and tensor potentials, $V^{(Central)}_{\lambda\lambda'}(r; J=0) = (V^{(0)}(r) - 3V^{(\sigma)}(r))_{\lambda\lambda'}$ for $J=0$, $V^{(Central)}_{\lambda\lambda'}(r; J=1) = (V^{(0)}(r) + V^{(\sigma)}(r))_{\lambda\lambda'}$, and $V^{(Tensor)}_{\lambda\lambda'}(r)$ for $J=1$, can be determined[1].

3 Comprehensive lattice QCD calculation with almost physical quark masses

$N_f = 2+1$ gauge configurations at almost the physical quark masses are used; they are generated on 96^4 lattice by employing the RG improved (Iwasaki) gauge action at $\beta = 1.82$ with the non-perturbatively $O(a)$ improved Wilson quark (clover) action at $(\kappa_{ud}, \kappa_s) = (0.126117, 0.124790)$ with

[1] The potential is obtained from the NBS wave function at moderately large imaginary time; it would be $t - t_0 \gg 1/m_\pi \sim$ 1.4 fm. In addition, no single state saturation between the ground state and the excited states with respect to the relative motion, e.g., $t - t_0 \gg (\Delta E)^{-1} = \left((2\pi)^2/(2\mu(La)^2)\right)^{-1} \simeq 8.0$ fm, is required for the HAL QCD method[9].

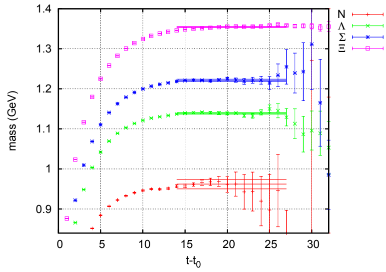

Figure 1. The effective mass of single baryon's correlation functions with utilising wall sources.

c_{sw} = 1.11 and the 6-APE stout smeared links with the smearing parameter $\rho = 0.1$. Preliminary studies show that the physical volume is $(aL)^4 \approx (8.1\text{fm})^4$ with the lattice spacing $a \approx 0.085$fm and $(m_\pi, m_K) \approx (146, 525)$MeV. See Ref.[18] for details on the generation of the gauge configuration. The periodic (Dirichlet) boundary condition is used for spacial (temporal) directions; wall quark source is employed with Coulomb gauge fixing which is separated from the Dirichlet boundary by $|t_{DBC} - t_0| = 48$. Forward and backward propagation in time are combined by using the charge conjugation and time reversal symmetries to double the statistics. Each gauge configuration is used four times by using the hypercubic SO(4, $\mathbb{Z}$) symmetry of 96^4 lattice. A large number of baryon-baryon potentials including the channels from NN to $\Xi\Xi$ are studied by means of HAL QCD method[11]. See also Ref.[17] for the thoroughgoing consistency check in the numerical outputs and comparison at various occasions between the UCA[19] and the present algorithm[16]. In this report, 96 wall sources are used for the 207 gauge configurations at every 10 trajectories. Statistical data are averaged with the bin size 23. Jackknife method is used to estimate the statistical errors.

4 Results

4.1 Effective masses from single baryons' correlation function

In the following analysis to obtain the potential, we use the single baryon's correlation functions, $(C_{B_1}(t-t_0)C_{B_2}(t-t_0))^{-1}$, instead of the simple exponential functional form $\mathrm{e}^{(m_{B_1}+m_{B_2})(t-t_0)}$ in order to calculate the normalised four-point correlation function. It would be beneficial to reduce the statistical noise because of the statistical correlation between the numerator and the denominator in the normalised four-point correlation function.

Fig. 1 shows the effective masses of the single baryon's correlation function. For the baryons N, Λ, and Σ, the plateaux start from the time slice around $t - t_0 \approx 14$. Therefore it is favourable that the potentials are obtained at the time slices $t - t_0 \gtrsim 14$. In this report we present preliminary results of potentials at time slices ($t - t_0 = 5 - 14$) of our on-going work.

4.2 ΣN ($I = 3/2$) system

4.2.1 Potentials

Fig. 2 shows the central potential in the $^3S_1 - ^3D_1$ (left), the tensor potential in the $^3S_1 - ^3D_1$ (centre), and the central potential in the $^1S_0$ (right) states of ΣN ($I = 3/2$) system, respectively. The stronger repulsive core of the central potential in the $^3S_1 - ^3D_1$ is seen in wider radial distance $r \lesssim 1$ fm; such a strong repulsion is consistent with quark model's prediction that is almost Pauli forbidden state in the flavor **10** representation. In addition, the central potential in the $^3S_1 - ^3D_1$ obtained at time slices $t - t_0 \geq 10$ shows small attractive well. The tensor potential is not as strong as the NN tensor

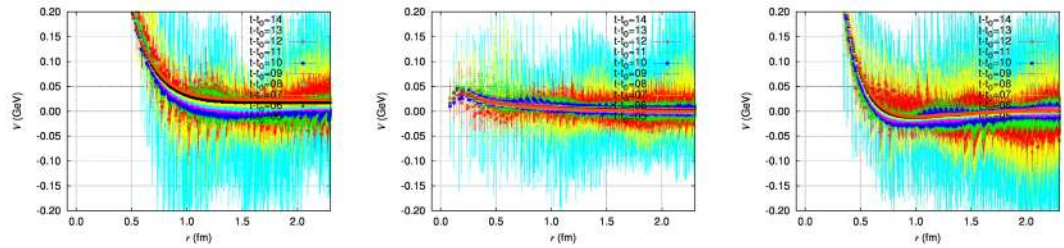

Figure 2. The ΣN potentials of ${}^3S_1 - {}^3D_1$ central (left), ${}^3S_1 - {}^3D_1$ tensor (centre), and ${}^1S_0$ central (right) in the $I = 3/2$ channel.

potential. The statistical fluctuation of the tensor potential becomes large at the time slices $t - t_0 \geq 11$ while that of the tensor potential at $t - t_0 \leq 10$ does not. These observations are consistent with the scattering phase shift calculated below. On the other hand, for the ${}^1S_0$ state the repulsive core of the central potential is relatively short ranged; the attractive force is seen in medium to long distance. This behaviour is similar to the NN ${}^1S_0$ because this state belongs to flavor **27**.

4.2.2 Scattering phase shifts

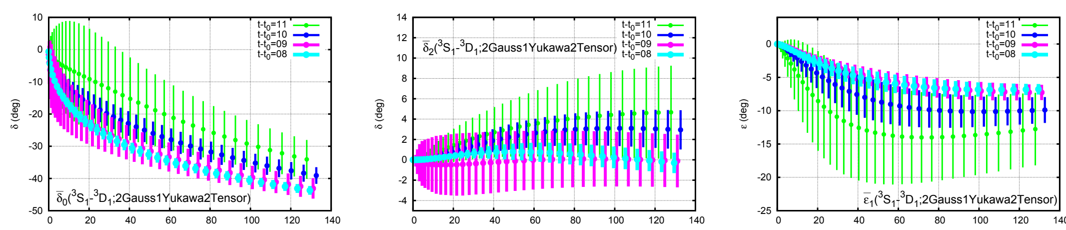

Figure 3. Scattering bar-phase shifts and mixing angle in the ${}^3S_1 - {}^3D_1$ states of $I = 3/2$ ΣN system, $\overline{\delta}_0$ (left), $\overline{\delta}_2$ (centre), and $\overline{\varepsilon}_1$ (right), obtained from parametrised functional form Eq. (8) by solving the Schrödinger equation.

The potential itself is not a physical observable. A reliable comparison with other results from experimental and/or theoretical (phenomenological) approaches should be made through physical observables, e.g., scattering phase shift. In order to obtain the scattering phase shift from present lattice QCD potential we first parametrise the potential with an analytic functional form. As the first attempt, we use following functional forms for the central and tensor potentials, respectively.

$$
\begin{aligned}
V_C(r) &= v_{C1} \mathrm{e}^{-\kappa_{C1} r^2} + v_{C2} \mathrm{e}^{-\kappa_{C2} r^2} + v_{C3} \left(1 - \mathrm{e}^{-\alpha_C r^2}\right)^2 \left(\frac{\mathrm{e}^{-\beta_C r}}{r}\right)^2, \\
V_T(r) &= v_{T1} \left(1 - \mathrm{e}^{-\alpha_{T1} r^2}\right)^2 \left(1 + \frac{3}{\beta_{T1} r} + \frac{3}{(\beta_{T1} r)^2}\right) \frac{\mathrm{e}^{-\beta_{T1} r}}{r} + v_{T2} \left(1 - \mathrm{e}^{-\alpha_{T2} r^2}\right)^2 \left(1 + \frac{3}{\beta_{T2} r} + \frac{3}{(\beta_{T2} r)^2}\right) \frac{\mathrm{e}^{-\beta_{T2} r}}{r}.
\end{aligned} \tag{8}
$$

Figure 3 shows the scattering phase shifts in ${}^3S_1 - {}^3D_1$ channels of $\Sigma N(I = 3/2)$ system obtained by solving the Schrödinger equation with above parametrised analytic functions. For the ${}^3S_1 - {}^3D_1$ channels, the scattering matrix is parametrised with three real parameters bar-phase shifts and mixing angle [20]:

$$S = \begin{pmatrix} e^{i\bar{\delta}_{J-1}} & 0 \\ 0 & e^{i\bar{\delta}_{J+1}} \end{pmatrix} \begin{pmatrix} \cos 2\bar{\varepsilon}_J & i\sin 2\bar{\varepsilon}_J \\ i\sin 2\bar{\varepsilon}_J & \cos 2\bar{\varepsilon}_J \end{pmatrix} \begin{pmatrix} e^{i\bar{\delta}_{J-1}} & 0 \\ 0 & e^{i\bar{\delta}_{J+1}} \end{pmatrix}. \tag{9}$$

The phase shift $\bar{\delta}_0$ at the time slices $t - t_0 = 9 - 11$ shows the interaction is repulsive while the phase shift $\bar{\delta}_2$ behaves around almost zero degree. Figure 4 shows the scattering phase shift in $^1S_0$ channel

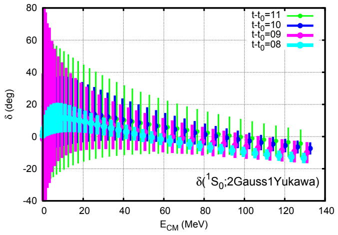

Figure 4. Scattering phase shift in the $^1S_0$ state of $I = 3/2$ ΣN system, obtained from parametrised functional form Eq. (8) by solving the Schrödinger equation.

of $\Sigma N(I = 3/2)$ system obtained through the above parametrised functions. The present result shows that the interaction in the $^1S_0$ channel of $\Sigma N(I = 3/2)$ system is attractive on average though the fluctuation is large especially for the time slices $t - t_0 = 9, 11$. The lattice potentials at flavor $SU(3)$ limit [21] show that group theoretical classification based on quark model works for clarifying the general behaviour of various baryon-baryon interactions in the S-wave; the ΣN $I = 3/2$ $^3S_1 -^3 D_1$ belongs to **10** which is almost Pauli forbidden while the ΣN $I = 3/2$ $^1S_0$ belongs to **27** which is same as NN $^1S_0$. The present S-wave (dominated) phase shifts, the repulsive (attractive) behaviour of $\bar{\delta}_0$ ($\delta(^1S_0)$), augur well for future quantitative conclusions with larger statistics. Incidentally, these behaviours are also qualitatively similar to recent studies [15, 22–24]. For both Figs. 3 and 4, the parametrisation procedure through the functional form may not be so stable at this moment especially for $t - t_0 = 11$. The present phase shifts and mixing angle should be regarded as preliminary results so that the large errorbars would be improved by future analysis with larger statistical data.

4.3 $\Lambda N - \Sigma N$ ($I = 1/2$) coupled-channel systems

Fig. 5 shows $\Lambda N - \Lambda N$ diagonal part for the central potential in the $^3S_1 -^3 D_1$ (left), the tensor potential in the $^3S_1 -^3 D_1$ (centre), and the central potential in the $^1S_0$ (right) states of $\Lambda N - \Sigma N$ ($I = 1/2$) system, respectively. There are repulsive cores in the short distance region and medium to long range attractive well for both central potentials. The relatively weak tensor potential is found. Fig. 6 shows $\Lambda N \to \Sigma N$ transition part for the central potential in the $^3S_1 -^3 D_1$ (left), the tensor potential in the $^3S_1 -^3 D_1$

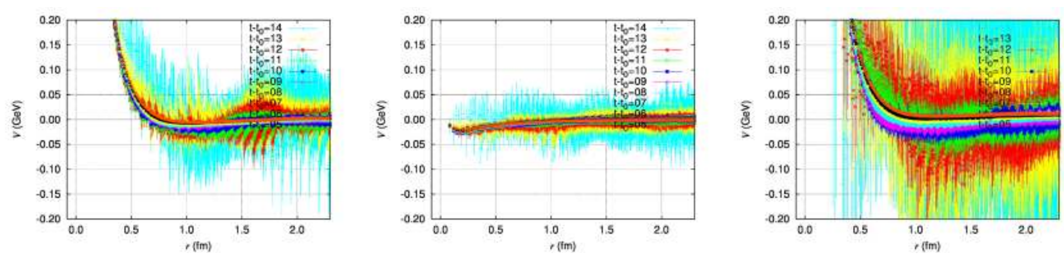

Figure 5. The $\Lambda N - \Lambda N$ potentials for $^3S_1 -^3 D_1$ central (left), $^3S_1 -^3 D_1$ tensor (centre), and $^1S_0$ central (right).

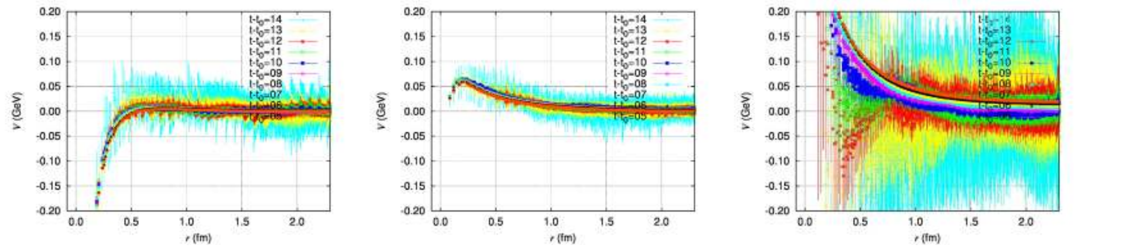

Figure 6. The $\Lambda N \to \Sigma N$ potentials for ${}^3S_1 - {}^3D_1$ central (left), ${}^3S_1 - {}^3D_1$ tensor (centre), and ${}^1S_0$ central (right).

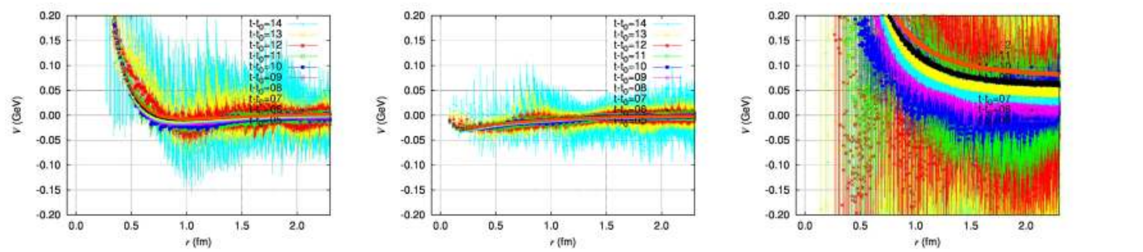

Figure 7. The $\Sigma N - \Sigma N$ potentials of ${}^3S_1 - {}^3D_1$ central (left), ${}^3S_1 - {}^3D_1$ tensor (centre), and ${}^1S_0$ central (right) in the $I = 1/2$ channel.

(centre), and the central potential in the ${}^1S_0$ (right) states of $\Lambda N - \Sigma N$ ($I = 1/2$) system, respectively. The ${}^3S_1 - {}^3D_1$ central potential is found to be short ranged. The tensor potential is not as strong as the NN tensor potential but it has sizable strength. The statistical fluctuation in the ${}^1S_0$ central potential is still large. Fig. 7 shows $\Sigma N - \Sigma N$ diagonal part for the central potential in the ${}^3S_1 - {}^3D_1$ (left), the tensor potential in the ${}^3S_1 - {}^3D_1$ (centre), and the central potential in the ${}^1S_0$ (right) states of $\Lambda N - \Sigma N$ ($I = 1/2$) system, respectively. There are short range repulsive core and medium range attractive well in the ${}^3S_1 - {}^3D_1$ central potential. The very strong repulsive core is seen in the ${}^1S_0$ central potential; it could be due to the large contribution of flavor $\mathbf{8}_s$ component, where we have $|\Sigma N\rangle = \frac{1}{\sqrt{10}}(3|\mathbf{8}_s\rangle - |\mathbf{27}\rangle)$ in the flavor SU(3) limit. The statistical fluctuation in the repulsive channel seems to be large.

5 Summary

In this report, the preliminary results of the ΛN, ΣN and their coupled-channel potentials are presented. For the ΣN ($I = 3/2$) interaction, phase shifts are calculated for the ${}^3S_1 - {}^3D_1$ and ${}^1S_0$ states. The phase shift $\bar{\delta}_0$ in the ${}^3S_1 - {}^3D_1$ channel shows that the ΣN ($I = 3/2, {}^3S_1$) interaction is repulsive. The phase shift in the ΣN ($I = 3/2, {}^1S_0$) channel shows that the interaction is attractive on average. These results are qualitatively consistent with recent phenomenological approaches. For the $\Lambda N - \Sigma N$ coupled-channel system, the potentials in the ${}^1S_0$ channel have still large statistical fluctuations because the number of statistics in the spin-singlet is factor 3 smaller than the number of statistics in the spin-triplet. In addition, large contribution from flavor $\mathbf{8}_s$ component in the ΣN ($I = 1/2$, ${}^1S_0$) could deteriorate the signal in the ΣN ${}^1S_0$ potential. Further calculations to obtain physical quantities with increased statistics are in progress and will be reported elsewhere.

We thank all collaborators in this project, above all, members of PACS Collaboration for the gauge configuration generation. The lattice QCD calculations have been performed on the K computer at RIKEN, AICS (hp120281, hp130023, hp140209, hp150223, hp150262, hp160211, hp170230), HOKUSAI FX100 computer at RIKEN, Wako (G15023, G16030, G17002) and HA-PACS at University of Tsukuba (14a-25, 15a-33, 14a-20, 15a-30). We thank ILDG/JLDG [25] which serves as an essential infrastructure in this study. This work is supported in part by MEXT Grant-in-Aid for Scientific Research (JP16K05340, JP25105505), and SPIRE (Strategic Program for Innovative Research) Field 5 project and "Priority issue on Post-K computer" (Elucidation of the Fundamental Laws and Evolution of the Universe) and Joint Institute for Computational Fundamental Science (JICFuS).

References

[1] O. Hashimoto, H. Tamura, Prog. Part. Nucl. Phys. **57**, 564 (2006)
[2] H. Nemura, Y. Akaishi, Y. Suzuki, Phys. Rev. Lett. **89**, 142504 (2002), nucl-th/0203013
[3] P. Demorest, T. Pennucci, S. Ransom, M. Roberts, J. Hessels, Nature **467**, 1081 (2010), 1010.5788
[4] J. Antoniadis et al., Science **340**, 6131 (2013), 1304.6875
[5] B. Abbott et al. (Virgo, LIGO Scientific), Phys. Rev. Lett. **119**, 161101 (2017), 1710.05832
[6] B.P. Abbott et al., Astrophys. J. **848**, L12 (2017), 1710.05833
[7] N. Ishii, S. Aoki, T. Hatsuda, Phys. Rev. Lett. **99**, 022001 (2007), nucl-th/0611096
[8] S. Aoki, T. Hatsuda, N. Ishii, Prog. Theor. Phys. **123**, 89 (2010), 0909.5585
[9] N. Ishii, S. Aoki, T. Doi, T. Hatsuda, Y. Ikeda, T. Inoue, K. Murano, H. Nemura, K. Sasaki (HAL QCD), Phys. Lett. **B712**, 437 (2012), 1203.3642
[10] S. Aoki, T. Doi, T. Hatsuda, Y. Ikeda, T. Inoue, N. Ishii, K. Murano, H. Nemura, K. Sasaki (HAL QCD), PTEP **2012**, 01A105 (2012), 1206.5088
[11] T. Doi et al., in *Proceedings, 35th International Symposium on Lattice Field Theory (Lattice2017): Granada, Spain*, to appear in EPJ Web Conf.; N. Ishii, et al., ibid.; K. Sasaki, et al., ibid.
[12] S. Gongyo et al. (2017), 1709.00654
[13] H. Nemura (HAL QCD), PoS **LATTICE2011**, 167 (2011), 1203.3320
[14] T. Iritani et al., JHEP **10**, 101 (2016), 1607.06371
[15] S.R. Beane, E. Chang, S.D. Cohen, W. Detmold, H.W. Lin, T.C. Luu, K. Orginos, A. Parreno, M.J. Savage, A. Walker-Loud, Phys. Rev. Lett. **109**, 172001 (2012), 1204.3606
[16] H. Nemura (HAL QCD), PoS **LATTICE2013**, 426 (2014)
[17] H. Nemura, Comput. Phys. Commun. **207**, 91 (2016), 1510.00903
[18] K.I. Ishikawa, N. Ishizuka, Y. Kuramashi, Y. Nakamura, Y. Namekawa, Y. Taniguchi, N. Ukita, T. Yamazaki, T. Yoshie (PACS), PoS **LATTICE2015**, 075 (2016), 1511.09222
[19] T. Doi, M.G. Endres, Comput. Phys. Commun. **184**, 117 (2013), 1205.0585
[20] H.P. Stapp, T.J. Ypsilantis, N. Metropolis, Phys. Rev. **105**, 302 (1957)
[21] T. Inoue et al. (HAL QCD Collaboration), Nucl.Phys. **A881**, 28 (2012), 1112.5926
[22] Y. Fujiwara, C. Nakamoto, Y. Suzuki, Phys. Rev. **C54**, 2180 (1996)
[23] I. Arisaka, K. Nakagawa, S. Shinmura, M. Wada, Prog. Theor. Phys. **104**, 995 (2000), [Erratum: Prog. Theor. Phys.107,237(2002)]
[24] J. Haidenbauer, S. Petschauer, N. Kaiser, U.G. Meissner, A. Nogga, W. Weise, Nucl. Phys. **A915**, 24 (2013), 1304.5339
[25] See [http://www.lqcd.org/ildg] and [http://www.jldg.org]